The Predictive Power of Computational Astrophysics as a Discovery Tool
Proceedings IAU Symposium No. 362, 2023
D. Bisikalo, D. Wiebe & C. Boily, eds.
doi:10.1017/S1743921322001296

Photoevaporation of Protoplanetary Disks

Ayano Komaki[1], Riouhei Nakatani[2] and Naoki Yoshida[1,3,4]

[1]Department of Physics, The University of Tokyo, 7-3-1 Hongo, Bunkyo, Tokyo 113-0033, Japan
email: ayano.komaki@phys.s.u-tokyo.ac.jp

[2]RIKEN Cluster for Pioneering Research, 2-1 Hirosawa, Wako-shi, Saitama 351-0198, Japan

[3]Kavli Institute for the Physics and Mathematics of the Universe (WPI), UT Institute for Advanced Study, The University of Tokyo, Kashiwa, Chiba 277-8583, Japan

[4]Research Center for the Early Universe (RESCEU), School of Science, The University of Tokyo, 7-3-1 Hongo, Bunkyo, Tokyo 113-0033, Japan

Abstract. Photoelectric effect of dust grains by UV radiation is an important process for disk heating, but as a disk evolves, the amount of dust grains decreases. Photoeaporation is a disk dispersal process, which is caused by high-energy radiation. We perform a set of photoevaporation simulations solving hydrodynamics with radiative transfer and non-equilibrium chemistry in a self-consistent way. We run a series of simulations with varying the dust-to-gas mass ratio in a range $\mathcal{D} = 10^{-1}$–10^{-8}. We show that H_2 pumping and X-ray heating mainly contribute to the disk heating in case of $\mathcal{D} \leq 10^{-3}$ and photoelectric effect mainly heats the gas in $\mathcal{D} \geq 10^{-3}$ cases. The mass-loss profile changes significantly with respect to the main heating process. The outer disk is more efficiently dispersed when photoelectric effect is the main heating source.

Keywords. protoplanetary disks, formation,hydrodynamics,pre–main-sequence

1. Introduction

Planets are formed inside protoplanetary disks (PPDs). Recent observations suggest that the protoplanetary disks disperse in a few Myr (Haisch 2001; Cieza 2007; Richert (2018)). The disk lifetime could be the time limit for planet formation. Planets move in the radial direction by interaction with the disk. This process is called migration. Clearly, the disk evolution and dispersal timescale determine the resulting planetary systems.

Accretion, magnetohydrodynamics (MHD) winds and photoevaporation are suggested to be main disk dispersal processes. Accretion is mass-loss onto the star by viscous evolution. Magnetorotational instability contributes to mass-loss by generating magnetorotational winds. MHD simulations show that this process is effective around a low-mass star. Photoevaporation is a process that the high-energy radiation (far-ultraviolet; FUV; $6\,\mathrm{eV} \leq h\nu < 13.6\,\mathrm{eV}$, extreme-ultraviolet; EUV; $13.6\,\mathrm{eV} \leq h\nu \leq 100\,\mathrm{eV}$, X-rays; $100\,\mathrm{eV} \leq h\nu$) from the central star heats the disk gas. The gas with sufficient kinetic energy eventually escapes from the system. EUV photons are absorbed by atomic hydrogen to form HII region and they do not reach the dense region. Since FUV and X-ray photons are absorbed by dust grains and various elements, they penetrate into a dense region of a disk and generate dense winds.

The dust properties are characterized by dust-to-gas mass ratio and size distribution. The dust size distribution is well explained as $\mathrm{d}n \propto a^{-3.5}\,\mathrm{d}a$, where a represents dust size. This is called MRN distribution (Mathis 1977). Dust grains in protoplanetary disks go through physical process such as dust sedimentation, dust growth and radial drift.

Recent SED observations by ALMA suggest that these process deplete small dust grains and change the dust size distribution (Espaillat 2014). Since small dust grains are the main cause of photoelectric heating, the heating rate of photoelectric effect is expected to decrease and temperature profile changes as the disk evolves. We characterize the amount of small dust grains with dust-to-gas mass ratio, $\mathcal{D}$ and perform a series of photoevaporation simulations varying $\mathcal{D}$ as a parameter.

The luminosity of FUV radiation is also known to decrease with disk evolution. We consider the effect on photoevaporation in this paper. The high-energy radiation is generated by chromosphere and accretion. The accretion rate is known to decrease with a timescale of $\sim 1\,\mathrm{Myr}$, and the lunimosity also decreases (Calvet & Gullbring 1998; Gullbring 1998). We perform a set of simulations with varying luminosity.

2. Methods

We solve hydrodynamics, radiative transfer and non-equilibrium chemistry in a a self-consistent way. We use PLUTO to solve hydrodynamics (Mignone 2007). We assume the disk is axisymmetric around the rotational axis, and symmetric with respect to the disk midplane. We perform 2D photoevaporation simulations with spherical coordinates (r, θ). In order to calculate the angular momentum, we consider 3D gas velocity, $v = (v_r, v_\theta, v_\phi)$. The equations we solve are

$$\frac{\partial \rho}{\partial t} + \nabla \cdot (\rho v) = 0, \tag{2.1}$$

$$\frac{\partial (\rho v_r)}{\partial t} + \nabla \cdot (\rho v_r v) = -\frac{\partial P}{\partial r} - \rho \frac{GM_*}{r^2} + \rho \frac{v_\theta^2 + v_\phi^2}{r}, \tag{2.2}$$

$$\frac{\partial (\rho v_\theta)}{\partial t} + \nabla \cdot (\rho v_\theta v) = -\frac{1}{r}\frac{\partial P}{\partial \theta} - \rho \frac{v_r v_\theta}{r} + \rho \frac{v_\phi^2}{r} \cot\theta, \tag{2.3}$$

$$\frac{\partial (\rho v_\phi)}{\partial t} + \nabla^l \cdot (\rho v_\phi v) = 0, \tag{2.4}$$

$$\frac{\partial E}{\partial t} + \nabla \cdot H v = -\rho v_r \frac{GM_*}{r^2} + \rho(\Gamma - \Lambda), \tag{2.5}$$

$$\frac{\partial n_{\mathrm{H}} y_i}{\partial t} + \nabla \cdot (n_{\mathrm{H}} y_i v) = n_{\mathrm{H}} R_i, \tag{2.6}$$

where ρ, P, M_*, y_i, R_i represent gas density, pressure, central stellar mass, abundance of each chemical species and reaction rate, respectively. Each of E, H, Γ, Λ expresses the energy, enthalpy, heating rate and cooling rate per unit volume, and G, n_{H} are the gravitational constant and the number density of elemental hydrogen.

We incorporate FUV, EUV, X-ray photons as radiation from the central star. We assume that the system is $\sim 1\,\mathrm{Myr}$ old, and determine each luminosity following Gorti & Hollenbach (2009). We incorporate EUV/X-ray photoionization heating, FUV photoelectric heating (Bakes & Tielens 1994), and heating by H_2 photodissociation and by H_2 pumping (Kuiper 2020; Nakatani 2021). We also incorporate dust-gas collisional cooling (Yorke & Welz 1996), fine-structure cooling of CII and OI (Hollenbach & McKee 1989; Osterbrock 1989; Santoro & Shull 2006), molecular line cooling of H_2 and CO (Galli & Palla 1998; Omukai *et al.* 2010), hydrogen Lyman α line cooling (Anninos 1997), and radiative recombination cooling (Spitzer 1978) as cooling sources. We take into account 10 chemical species, HI, HII, H^-, HeI, H_2, H_2^+, CO, OI, CII and electrons.

We calculate the dust temperature in the following manner. We incorporate both the direct and diffuse radiation to solve the dust temperature. We perform ray-tracing for the direct component and adopt the flux-limited-diffusion (FLD) approximation for the diffused component (Kuiper 2010; Kuiper & Klessen 2013; Kuiper 2020).

https://doi.org/10.1017/S1743921322001296 Published online by Cambridge University Press

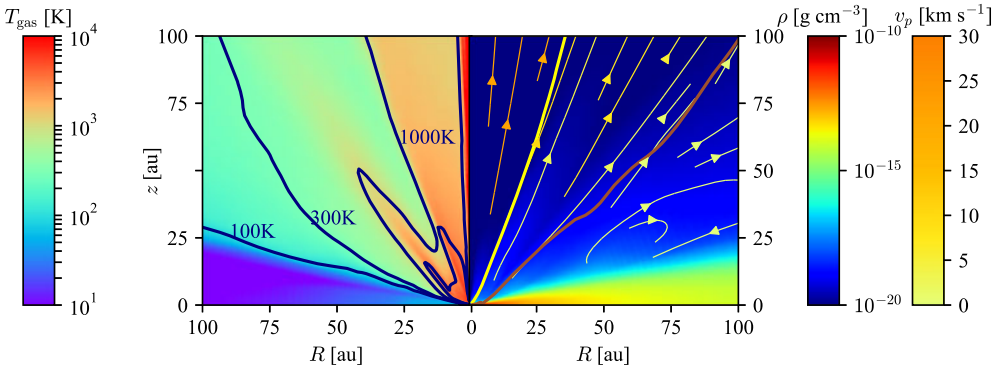

Figure 1. The disk structure of the simulation with $\mathcal{D} = 10^{-6}$. The color map on the left portion shows the gas temperature, $T_{\rm gas}$, and the right portion shows the density distribution, ρ. The right portion also shows the distribution of H-bearing species. The yellow line on the right side represents the ionization front where the abundance of HII is 0.5, and the brown line indicates the dissociation front where the abundance of H_2 is 0.25.The navy contour lines on the left side represent where the gas temperature is 100 K, 300 K, 1000 K, and 3000 K. The arrows represent the poloidal velocity of the gas, which is defined as $v_p = \sqrt{v_r^2 + v_\theta^2}$. For clarity, we do not plot the arrows where the velocity is less than 0.1km s^{-1}, which are mostly in the optically thick disk region.

We define the computational domain of the polar angle to $[0,\ \pi/2]$, and the radial coordinate to $[0.1r_{\rm g},\ 20r_{\rm g}]$. The gravitational radius $r_{\rm g}$ is defined as

$$r_{\rm g} = \frac{GM_*}{(10{\rm km\,s^{-1}})^2} \simeq 8.87\ {\rm au} \left(\frac{M_*}{1\ {\rm M}_\odot}\right).$$

for a fully ionized gas with $T_{\rm gas} = 10^4$ K. We assume that the disk mass is 3% of the central stellar mass i.e., $M_{\rm disk} = 0.03M_*$ (Andrews & Williams 2005). See Nakatani (2018a,b) and Komaki (2021) for more details.

3. Results

Fig. 1 shows the time-averaged simulation snapshot with $\mathcal{D} = 10^{-6}$. We average from 840 yr to 5000 yr to avoid the effect of the initial condition and transient fluctuations. Averaging over time smoothes out short-period fluctuations of the mass-loss rates. EUV radiation heats the gas near the central star and at high latitudes. The gas forms the HII region there. The gas temperature is lowered via adiabatic cooling and becomes $T_{\rm gas} \sim 3000$ K. The HI region and H_2 region are formed at the lower latitudes. FUV photoelectric effect effectively heats the HI region up to $\gtrsim 3000$ K for $\mathcal{D} \geq 10^{-2}$. In the case of $\mathcal{D} = 10^{-3}$, the main heating source is also FUV photoelectric effect, but the gas is cooled by OI line emission down to $\lesssim 3000$ K. In the runs with $\mathcal{D} = 10^{-4}$–10^{-8}, the photoelectric heating by FUV radiation is weak, therefore the thermochemical structure is different from the high $\mathcal{D}$ cases. X-ray radiation is the main heating source instead of FUV photoelectric effect in the HI region. The gas temperature is efficiently lowered by adiabatic cooling and OI line emission down to 300 K.

The FUV photoelectric heating rate decreases as the dust-to-gas mass ratio becomes smaller, following $\Gamma_{\rm FUV} \propto \mathcal{D}$. In the runs with $\mathcal{D} = 10^{-1}$–10^{-2}, the disk gas is dominantly heated by FUV photoelectric effect, while in the run with $\mathcal{D} = 10^{-3}$, the heating rate for FUV photoelectric effect becomes almost same as the heating rates for X-ray radiation and H_2 pumping. In case of $\mathcal{D} < 10^{-3}$, the disk gas is heated mainly by X-ray radiation and H_2 pumping. The heating rate by H_2 pumping is highest at the H_2 dissociation front.

https://doi.org/10.1017/S1743921322001296 Published online by Cambridge University Press

The pumped H_2 molecules heat the gas by collisions with HI or H_2. H_2 pumping heats the gas effectively in a dense region whose density is higher than the critical density, $\rho \sim 5.0 \times 10^{-20}\,\mathrm{g\,cm^{-3}}$. H_2 pumping heating becomes relatively important at the inner region. H_2 pumping has a few times higher heating rate than X-ray heating at the H_2 dissociation front. In the inner region with $r \sim 10 r_\mathrm{g}$, H_2 pumping heating rate is higher than X-ray heating. The ratio becomes ~ 300 at the innermost region. In contrast, in the outer regions, H_2 pumping has a heating rate a few times lower than X-ray heating. The whole thermochemical structure is determined by both H_2 pumping and X-ray heating. The disk gas temperature is 200–300 K at $r = 10 r_\mathrm{g}$, and this is lower by a factor of ~ 1.5–2 than the fiducial $\mathcal{D}$ case.

We calculate the mass-loss rate from the whole disk based on the simulation results using

$$\dot{M} = \int_{S,\eta>0} \rho v \cdot dS, \tag{3.1}$$

where dS represents the surface unit area at $r = 100$ au. We define η as the total enthalpy and it is calculated by

$$\eta = \frac{1}{2} v_p^2 + \frac{1}{2} v_\phi^2 + \frac{\gamma}{\gamma - 1} c_\mathrm{s}^2 - \frac{GM_*}{r}.$$

We define $v_p = \sqrt{v_r^2 + v_\theta^2}$ as the poloidal velocity, γ as the specific heat ratio, and c_s as the sound velocity. We assume that only the gas satisfying $\eta > 0$ escapes from the system eventually.

Based on Fig. 2a, we classify the disk dispersal by the difference of the disk heating profile.

$$\dot{M} = \begin{cases} 1.0 \times 10^{-9} \times 10^{-0.15\mathcal{D}^2 - 0.49\mathcal{D}}\,\mathrm{M_\odot\,yr^{-1}} & (\mathcal{D} \geq 10^{-3}) \\ 5.6 \times 10^{-10}\,\mathrm{M_\odot\,yr^{-1}} & (\mathcal{D} \leq 10^{-5}) \end{cases}.$$

In the run with $\mathcal{D} = 10^{-1}$, the disk is optically thick because of abundant dust grains. The photoevaporative flows are launched from the region with lower density, which result in the lower mass-loss rate compared to $\mathcal{D} = 10^{-2}$ case. When the dust-to-gas mass ratio is $\mathcal{D} \leq 10^{-4}$, the gas temperature is raised by H_2 pumping and X-ray heating. Since the abundance of H_2 does not depend on the dust amount, we expect that the mass-loss rate with even lower dust-to-gas mass ratio would stay constant. In the cases of $\mathcal{D} = 10^{-6}$–10^{-8}, the mass-loss rate converges to $\dot{M} \sim 5$–$6 \times 10^{-10}\,\mathrm{M_\odot\,yr^{-1}}$.

4. Implications

Observations suggest that the luminosity of high-energy radiation differs among the same spectral type stars (Gullbring 1998; Vidotto 2014). Accretion rate decreases as the disk evolves (Hartmann 1998). Since high-energy radiation is generated by accretion shock, the luminosity also decreases with disk evolution. The FUV luminosity decreases with the accretion rate following $L_\mathrm{FUV} \propto \dot{M}_\mathrm{acc}$ (Calvet & Gullbring 1998; Gullbring 1998). Considering the accretion rate decays following $t^{-3/2}$, L_FUV drops to $0.1 L_\mathrm{FUV,f}$ in ~ 3 Myr, where $L_\mathrm{FUV,f} = 10^{31.7}\,\mathrm{erg\,s^{-1}}$ is a fiducial value of a $1\,\mathrm{M_\odot}$ star. Komaki (2021) suggest that among FUV and X-ray photons, the photons with higher luminosity become the main heating source of the disk gas and generate photoevaporative flows. The change of the luminosity could affect the main heating process and mass-loss by photoevaporation. In $\mathcal{D} = 10^{-2}$–10^{-6} cases, we perform a set of photoevaporation simulations varying FUV luminosity as a parameter with $L_\mathrm{FUV} = 0.1 L_\mathrm{FUV,f}, 10 L_\mathrm{FUV,f}$. We set X-ray luminosity as a constant value, $L_\mathrm{X\text{-}ray} = 10^{30.4}\,\mathrm{erg\,s^{-1}}$.

https://doi.org/10.1017/S1743921322001296 Published online by Cambridge University Press

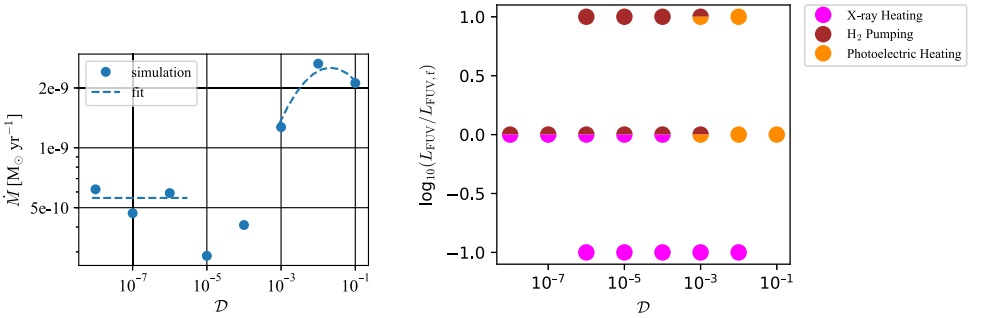

(a) The time-averaged mass-loss rate for each dust-to-gas mass ratio.

(b) The main heating process is plotted for each run varying $\mathcal{D}$ and $L_{\rm FUV}$.

Figure 2. (a) shows the time-averaged mass-loss rate for each dust-to-gas mass ratio. The blue dots represent the simulation results. The dotted line is a fit. (b) shows the main heating process, plotted for each run varying $\mathcal{D}$ and $L_{\rm FUV}$. The orange, brown and magenta represent photoelectric heating, heating by H_2 pumping and X-ray heating. $L_{\rm FUV,f}$ expresses the fiducial FUV luminosity.

Fig. 2b shows the main heating process in our simulation set. When the luminosity satisfies $L_{\rm FUV} < L_{\rm X\text{-}ray}$, X-ray radiation mainly heats the disk gas regardless of the dust-to-gas mass ratio. When the luminosity satisfies $L_{\rm FUV} > L_{\rm X\text{-}ray}$, the gas temperature is heated mainly by FUV radiation. Especially in case of $\mathcal{D} \leq 10^{-3}$, H_2 pumping becomes the main heating process while in case of $\mathcal{D} \geq 10^{-3}$, the gas is heated by photoelectric effect. As a disk evolves, small dust grains and FUV luminosity both decreases. As shown in the previous section, the temperature structure depends on the disk heating process. The mass-loss profile also changes with the temperature structure. The disk surface mass-loss rate is also suggested to vary with a disk evolution.

5. Discussion

Q1: Can a photoevaporation blow away a dust?

A: Hutchison (2016) performed a simulation and show that dust grains smaller than 0.3 μm are blown up by photoevaporative winds.

Q2: Does dust photoevaporation correlate with gas mass-loss photoevaporation?

A: Yes. Since the dust photoevaporation is dependent on the gas velocity, I think dust photoevaporation rate depends on the gas photoevaporation rate.

Q3: What is the roles of EUV and X-ray radiation?

A: The HII region is formed in the low-polar-angle region. EUV photons heat the gas effectively only in this region and do not contribute to the disk heating. As for X-ray radiation, X-ray is not the main heating source, but contribute to mass-loss. In $M_* = 3\,{\rm M}_\odot$ case, the mass-loss rate is lower than other cases because of the low X-ray luminosity. This shows that X-ray radiation contribute to the photoevaporation to some extent.

References

Andrews, Sean M. & Williams, Jonathan P. 2005, *ApJ*, 631, 1134
Anninos, Peter and Zhang, Yu and Abel, Tom and Norman, Michael L. 1997, *NewA*, 2, 209

https://doi.org/10.1017/S1743921322001296 Published online by Cambridge University Press

Bakes, E. L. O. and Tielens, A. G. G. M. 1994, *ApJ*, 427, 822
Calvet, Nuria and Gullbring, Erik 1998, *ApJ*, 509, 802
Cieza, Lucas and Padgett, Deborah L. and Stapelfeldt, Karl R. and Augereau, Jean-Charles and Harvey, Paul and Evans, Neal J., II and Merín, Bruno and Koerner, David and Sargent, Anneila and van Dishoeck, Ewine F. and Allen, Lori and Blake, Geoffrey and Brooke, Timothy and Chapman, Nicholas and Huard, Tracy and Lai, Shih-Ping and Mundy, Lee and Myers, Philip C. and Spiesman, William and Wahhaj, Zahed 2007, *ApJ*, 667, 308
Espaillat, C. and Muzerolle, J. and Najita, J. and Andrews, S. and Zhu, Z. and Calvet, N. and Kraus, S. and Hashimoto, J. and Kraus, A. and D'Alessio, P. 2014, *Protostars and Planets VI*
Galli, Daniele and Palla, Francesco 1998, *AAP*, 335, 403
Gorti, U. and Hollenbach, D. 2009, *ApJ*, 690, 1539
Gullbring, Erik and Hartmann, Lee and Briceño, Cesar and Calvet, Nuria 1993, *ApJ*, 492, 323
Haisch, Karl E., Jr. and Lada, Elizabeth A. and Lada, Charles J. 2001, *ApJL*, 553, L153
Hartmann, Lee and Calvet, Nuria and Gullbring, Erik and D'Alessio, Paola 1998, *ApJ*, 495, 385
Hollenbach, David and McKee, Christopher F. 1989, *ApJ*, 342, 306
Komaki, Ayano and Nakatani, Riouhei and Yoshida, Naoki 2021, *ApJ*, 910, 51
Kuiper, R. and Klahr, H. and Dullemond, C. and Kley, W. and Henning, T. 2010, *AAP*, 511, A81
Kuiper, R. and Klessen, R. S. 2013, *AAP*, 555, A7
Kuiper, Rolf and Yorke, Harold W. and Mignone, Andrea 2020, *ApJS*, 250, 13
Mathis, J. S. and Rumpl, W. and Nordsieck, K. H. 1977, *ApJ*, 217, 425M
Mignone, A. and Bodo, G. and Massaglia, S. and Matsakos, T. and Tesileanu, O. and Zanni, C. and Ferrari, A. 2007, *ApJS*, 170, 228
Nakatani, Riouhei and Hosokawa, Takashi and Yoshida, Naoki and Nomura, Hideko and Kuiper, Rolf 2018, *ApJ*, 857, 57
Nakatani, Riouhei and Hosokawa, Takashi and Yoshida, Naoki and Nomura, Hideko and Kuiper, Rolf 2018, *ApJ*, 865, 75
Nakatani, Riouhei and Kobayashi, Hiroshi and Kuiper, Rolf and Nomura, Hideko and Aikawa, Yuri 2021, *ApJ*, 915, 90
Osterbrock, Donald E. 1989, *University Science Books*
Omukai, Kazuyuki and Hosokawa, Takashi and Yoshida, Naoki 2010, *ApJ*, 722, 1793
Ribas, Álvaro and Bouy, Hervé and Merín, Bruno 2015, *AAP*, 576, A52
Richert, A. J. W. and Getman, K. V. and Feigelson, E. D. and Kuhn, M. A. and Broos, P. S. and Povich, M. S. and Bate, M. R. and Garmire, G. P. 2018, *MNRAS*, 477, 5191R
Santoro, Fernando and Shull, J. Michael 2006, *ApJ*, 643, 26
Spitzer, Lyman 1978, *Physical processes in the interstellar medium (Wiley-Interscience)*
Vidotto, A. A. and Gregory, S. G. and Jardine, M. and Donati, J. F. and Petit, P. and Morin, J. and Folsom, C. P. and Bouvier, J. and Cameron, A. C. and Hussain, G. and Marsden, S. and Waite, I. A. and Fares, R. and Jeffers, S. and do Nascimento, J. D. 2014, *MNRAS*, 441, 2361
Yorke, H. W. and Welz, A. 1996, *AAP*, 315, 555